RESEARCH ARTICLE SUMMARY

PROTEOMICS

Tracking cancer drugs in living cells by thermal profiling of the proteome

Mikhail M. Savitski,[1]* Friedrich B. M. Reinhard,[1] Holger Franken,[1] Thilo Werner,[1] Maria Fälth Savitski,[1] Dirk Eberhard,[1] Daniel Martinez Molina,[2] Rozbeh Jafari,[2] Rebecca Bakszt Dovega,[2] Susan Klaeger,[3,4] Bernhard Kuster,[3,4] Pär Nordlund,[2,5] Marcus Bantscheff,[1]* Gerard Drewes[1]*

INTRODUCTION: Understanding drug mechanism poses the daunting challenge of determining the affinity of the drug for all potential targets. Drug target engagement can be assessed by means of a cellular thermal shift assay (CETSA) based on ligand-induced changes in protein thermal stability. We combined the CETSA method with quantitative mass spectrometry to study the effect of drugs on the thermal profile of a cellular proteome comprising more than 7000 proteins. The approach enabled the monitoring of drug targets and downstream effectors.

RATIONALE: We devised a method for the thermal profiling of cellular proteomes. Cells were cultured with or without drugs and heated to different temperatures so as to induce protein denaturation, and remaining soluble proteins were extracted with buffer. At each temperature, soluble proteins were quantified by means of high-resolution mass spectrometry, yielding denaturation curves. This allowed determination of thermal stability and the identification of ligand-induced shifts. To rank binding affinities among multiple targets, we determined stability profiles across a range of compound concentrations at a defined temperature. Comparison of the thermal profiles obtained after drug treatment of intact cells versus cell extract allowed us to distinguish effects induced by ligand binding from those induced by downstream modifications.

RESULTS: We performed thermal proteome profiling (TPP) on human K562 cells by heating intact cells or cell extracts and observed marked differences in melting properties between the two settings, with a trend toward increased protein stability in cell extract. Adenosine triphosphatase (ATP)–binding proteins showed a significant trend toward increased stability in intact cells, suggesting stabilization by the endogenous ligand. This was confirmed with the addition of ATP to cell extract, which resulted in increased stability for this protein group. The ability of TPP to identify target binding was validated by using the broad-specificity inhibitors staurosporine and GSK3182571, which induced shifts in the melting temperatures of many kinase targets and also affected the thermal profiles of other proteins, including regulatory subunits of kinase complexes. We identified the heme biosynthesis enzyme ferrochelatase (FECH) as an off-target of several kinase inhibitors and showed that the drug vemurafenib reaches full target occupancy of its cognate target BRAF and the off-target FECH within a narrow concentration window. FECH deficiency is genetically linked to protoporphyria, suggesting that the photosensitivity induced by vemurafenib and other drugs is mediated by FECH. Drug treatment of live cells affected not only direct target proteins but also downstream effectors. The ABL inhibitor dasatinib induced thermal shifts in several proteins downstream of BCR-ABL, including CRKL, and at concentrations in good agreement with the effect on cell growth.

ON OUR WEB SITE

Read the full article at http://dx.doi.org/10.1126/science.1255784

CONCLUSION: Thermal profiling of cellular proteomes enables the differential assessment of protein ligand binding and other protein modifications, providing an unbiased measure of drug-target occupancy for multiple targets and facilitating the identification of markers for drug efficacy and toxicity. ■

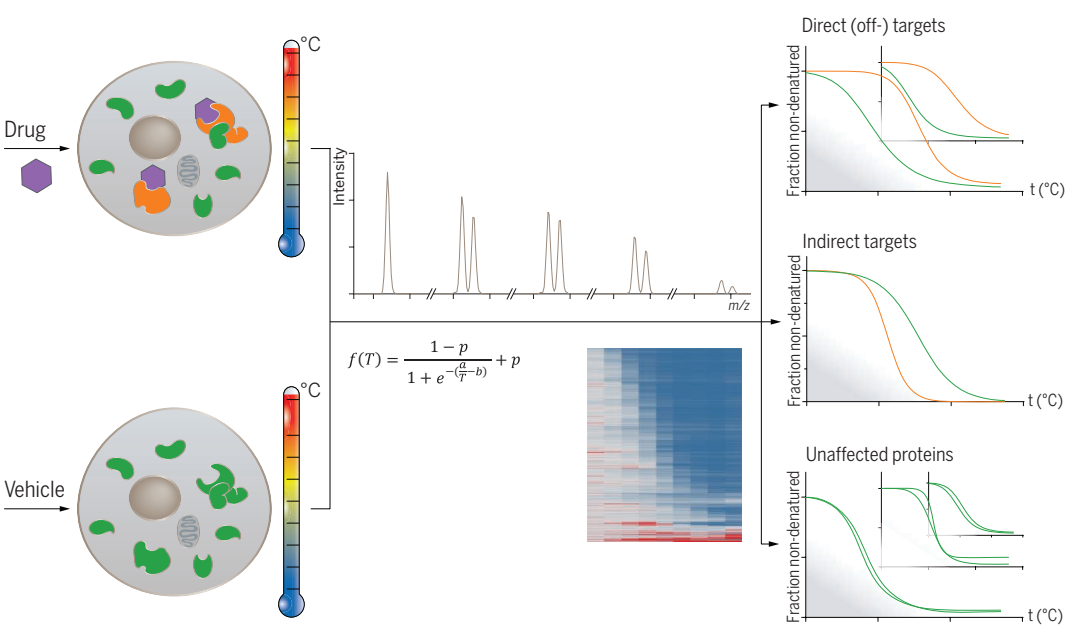

Tracking drugs in living cells. Drugs alter the thermal stability of proteins directly through compound binding or indirectly through changes in overall protein state. Thermal proteome profiling determines melting curves for thousands of proteins and tracks drug action in cells.

[1]Cellzome GmbH, Molecular Discovery Research, GlaxoSmithKline, Meyerhofstrasse 1, Heidelberg, Germany.
[2]Division of Biophysics, Department of Medical Biochemistry and Biophysics, Karolinska Institutet, Stockholm, Sweden.
[3]Department of Proteomics and Bioanalytics, Technische Universität München, Emil Erlenmeyer Forum 5, Freising, Germany.
[4]German Cancer Consortium, German Cancer Research Center, Heidelberg, Germany.
[5]Centre for Biomedical Structural Biology, Nanyang Technological University, Singapore.
*Corresponding author. E-mail: mikhail.m.savitski@gsk.com (M.M.S.); marcus.x.bantscheff@gsk.com (M.B.); gerard.c.drewes@gsk.com (G.D.)
Cite this article as: M. M. Savitski *et al.*, *Science* **346**, 1255784 (2014). DOI: 10.1126/science.1255784

RESEARCH ARTICLE

PROTEOMICS

Tracking cancer drugs in living cells by thermal profiling of the proteome

Mikhail M. Savitski,[1]*† Friedrich B. M. Reinhard,[1]† Holger Franken,[1] Thilo Werner,[1] Maria Fälth Savitski,[1] Dirk Eberhard,[1] Daniel Martinez Molina,[2] Rozbeh Jafari,[2] Rebecca Bakszt Dovega,[2] Susan Klaeger,[3,4] Bernhard Kuster,[3,4] Pär Nordlund,[2,5] Marcus Bantscheff,[1]* Gerard Drewes[1]*

The thermal stability of proteins can be used to assess ligand binding in living cells. We have generalized this concept by determining the thermal profiles of more than 7000 proteins in human cells by means of mass spectrometry. Monitoring the effects of small-molecule ligands on the profiles delineated more than 50 targets for the kinase inhibitor staurosporine. We identified the heme biosynthesis enzyme ferrochelatase as a target of kinase inhibitors and suggest that its inhibition causes the phototoxicity observed with vemurafenib and alectinib. Thermal shifts were also observed for downstream effectors of drug treatment. In live cells, dasatinib induced shifts in BCR-ABL pathway proteins, including CRK/CRKL. Thermal proteome profiling provides an unbiased measure of drug-target engagement and facilitates identification of markers for drug efficacy and toxicity.

The complete determination of the proteomic state of a cell, referred to as the proteotype, links genotype and the cellular phenotype. Thus, the proteotype of the target cell or tissue represents an important context for the study of drug action. However, the task of accurately describing a proteotype remains daunting because of the inherent complexity of the proteome, comprising in excess of 10,000 gene products expressed at levels differing over six or more orders of magnitude, many of which occur in different splice isoforms and with different posttranslational modifications at different subcellular localizations (*1*). Current expression proteomics methods describe proteotypes as lists of proteins and semiquantitative expression levels (*2*). In addition, there are methods for the cell-wide assessment of some but not all post-translational modifications (*3*, *4*). Studies focused on the mechanism of bioactive compounds, such as small-molecule drugs or peptides, frequently rely on affinity-based enrichment strategies to identify prospective binding partners from a cell extract (*5*–*7*). These approaches can be combined for the differential study of cellular phenotypes—for instance, the status of signaling pathways or for biomarker discovery (*8*, *9*). However, unbiased approaches for the cell-wide assessment of protein state and protein function are not available.

Changes in the thermal stability of proteins are frequently used to study ligand binding (*10*, *11*) and, with the recent development of the cellular thermal shift assay (CETSA), can now be observed in living cells (*12*), enabling the monitoring of target engagement, which is a key parameter in drug discovery (*13*). We extended this approach to address two challenges critical in drug discovery: target and off-target identification and discovery of molecular biomarkers for drug efficacy. By combining the CETSA method with multiplexed quantitative mass spectrometry (MS), we established the proteome-wide determination of protein thermal stability in intact cells as an independent and complementary strategy for the characterization of cellular proteotypes. Our approach, termed "thermal proteome profiling," includes but is not limited to the monitoring of protein-ligand interactions directly in cells or tissues because in theory, any modification of a protein can affect its thermal stability (*14*). Here, we demonstrate that monitoring thermal stability across cellular proteomes in different states, such as under drug treatment, enables the identification of direct physical interaction partners and downstream effectors as markers of target engagement and drug efficacy.

Proteome-wide profiling of protein thermal stability

To monitor the thermal stability of proteins across 10 different temperatures, we used the recently developed neutron-encoded isobaric mass tagging reagents (TMT10) (*15*) in conjunction with high-resolution MS. This allowed acquisition of full melting curves for a large proportion of expressed soluble proteins in a single liquid chromatography–MS (LC-MS)/MS experiment. In a typical experiment, cells were cultured under differential conditions, such as drug treatment (Fig. 1). For each condition, the cells were divided into 10 aliquots, each of which was briefly heated to a different temperature followed by extraction with phosphate-buffered saline (PBS). Around their intrinsic melting temperature, proteins in the cell denature and subsequently aggregate (*16*), resulting in their gradual disappearance from the PBS-extracted samples with increasing temperatures (*12*, *17*). This protocol is only suitable for the soluble fraction of the proteome because membrane proteins are not solubilized under these conditions. After extraction, each sample was trypsinated and labeled with a different isotope-coded isobaric mass tag (*15*), and the 10 samples from each condition were mixed and analyzed by means of LC-MS/MS. The reporter ion intensities acquired in the MS/MS fragment spectra were used to fit a curve and calculate a specific melting temperature (T_m) for each protein, which was then compared between the vehicle-treated and drug-treated samples. The resulting curves that display the increase in protein aggregation with temperature in many cases directly reflect the underlying unfolding or "melting" event. For many proteins, a good correlation between the thermofluor unfolding assay and heat-induced precipitation in solution, or in cells by CETSA, has been demonstrated (*11*, *17*), suggesting that properly shaped curves represent real unfolding events. Hence, ligand-induced curve shifts indicate a change in the thermal stability of the protein rather than a change in the aggregation properties. In a variation of the cell-based protocol, thermal stability can also be assessed in a cell extract. This alternative strategy avoids the separate extraction of each cell sample, potentially allows more controlled conditions (*12*), and in conjunction with cell treatment experiments, enables distinguishing T_m shifts induced by ligand binding from those induced by downstream modifications.

The thermal profile of a cellular proteome

We acquired quantitative thermal stability data for 5299 proteins across 10 different temperatures from the human K562 chronic myeloid leukemia cell line. This data set could be regarded as the first description of the melting proteome ("meltome") of a human cell. Thermal profiles were acquired in two experimental settings in which either intact cells or cell extracts were heated. In both settings, we noted a weak but significant anticorrelation of the thermal stability with molecular weight because smaller proteins tend to be more stable (fig. S1). A comparison of the thermal stability across a set of 3204 proteins robustly quantified in both intact cells and cell extract revealed marked differences in melting properties between cells and extract (Fig. 2 and table S1). Hierarchical cluster analysis of the temperature-dependent relative protein concentrations in the heated cell samples revealed a group of proteins that exhibited an increase in concentration at ~50°C, followed by a pronounced decrease at ~56°C, and another group of proteins with a concentration increase at ~63°C.

[1]Cellzome GmbH, Molecular Discovery Research, GlaxoSmithKline, Meyerhofstrasse 1, Heidelberg, Germany. [2]Division of Biophysics, Department of Medical Biochemistry and Biophysics, Karolinska Institutet, Stockholm, Sweden. [3]Department of Proteomics and Bioanalytics, Technische Universität München, Emil Erlenmeyer Forum 5, Freising, Germany. [4]German Cancer Consortium, German Cancer Research Center, Heidelberg, Germany. [5]Centre for Biomedical Structural Biology, Nanyang Technological University, Singapore.
*Corresponding author. E-mail: mikhail.m.savitski@gsk.com (M.M.S.); marcus.x.bantscheff@gsk.com (M.B.); gerard.c.drewes@gsk.com (G.D.) †These authors contributed equally to this work.

The concentration increases observed at these temperatures indicate increased solubilization at the initial temperatures followed by aggregation at higher temperatures. Gene ontology analysis indicated that the proteins in these clusters are released from disintegrating organelles (such as mitochondria) or large protein assemblies (such as ribosomes) (Fig. 2A and fig. S2). When cell extract rather than intact cells was heated, we did not observe any substantial increases in protein concentration by heating, likely because of the disruption of cellular structures during cell lysis. Melting points were determined for proteins passing curve-fitting quality criteria as described in the supplementary materials, materials and methods (Fig. 2B). On average, proteins showed 2.7°C higher T_m values in cell extract as compared with intact cells. Although this difference is significant (SEM = 0.06°C, $P < 0.01$, t test), the correlation of melting points acquired in cell extracts and intact cell experiments (R^2 = 0.3) is considerably lower than the correlation of the respective replicate experiments (intact cell, R^2 = 0.93; cell extract, R^2 = 0.89), suggesting that the disruption of the cellular context heterogeneously affects protein stability (Fig. 2B). The global trend of increased protein stability in cell extract suggests an effect on protein precipitation due to lower protein concentrations in cell extract as compared with intact cells. This contrasts with the hypothesis that molecular crowding in the cytosol should exert a stabilizing effect, which was based on the observation that phosphoglycerate kinase exhibits increased stability inside the cell (*18*). This is in line with our data for this protein but could also be explained by a stabilizing effect of the endogenous cosubstrate adenosine 5′-triphosphate (ATP) (fig. S3). We speculated that proteins that are bound to a ligand inside the cell might show an increase in thermal stability contrary to the general trend because the dissociation of protein-ligand complexes during extraction would result in their destabilization. This hypothesis was substantiated by an analysis of the T_m values of a set of 440 proteins annotated as ATP binders, which showed a significant trend ($P < 0.01$, t test) toward increased stability in intact cells when compared with all other proteins (table S2). This was experimentally confirmed with the determination of thermal shifts induced by the addition of MgATP to a K562 cell extract at approximately physiological concentrations (2 mM) (*19*). In these thermal profiles, we detected 213 proteins annotated as ATP binders that in two independent replicates showed the predicted trend toward increased stability upon addition of ATP, whereas all other proteins detected in these experiments did not show this trend (fig. S4 and table S3). Further analysis of the thermal proteome profiles revealed that proteins categorized as DNA binders were enriched in the set with the lowest melting points, suggesting that these proteins were extracted without their DNA ligand. Indeed, the DNA-binding properties of proteins can be assessed by adding DNA fragments to the cell extract. This is exemplified by p53, the global transcription regulator for stress. Wild-type p53 was stabilized upon addition of its cognate effector DNA, whereas the p53 R273H mutant that does not bind these effector sequences (*20*) was not stabilized (fig. S5). These results demonstrate the potential of thermal proteome profiling for the large-scale analysis of proteome-ligand interactions, including endogenous ligands such as cofactors or metabolites.

Monitoring of drug effects on thermal proteome profiles

The analysis of drug mechanism of action by profiling both targeted and off-target protein binding will likely represent a major application of thermal proteome profiling. As a proof of principle, we studied kinase inhibitors because kinases are an important target class, with key regulatory functions in cellular pathways. An important question in drug target identification is the prevalence of false-positive and false-negative identifications. To investigate the reliability of thermal proteome profiling, we selected two structurally divergent promiscuous kinase inhibitors with a known spectrum of targets, staurosporine and GSK3182571, which is a close analog of CTx-0294885 (*21*). Profiles

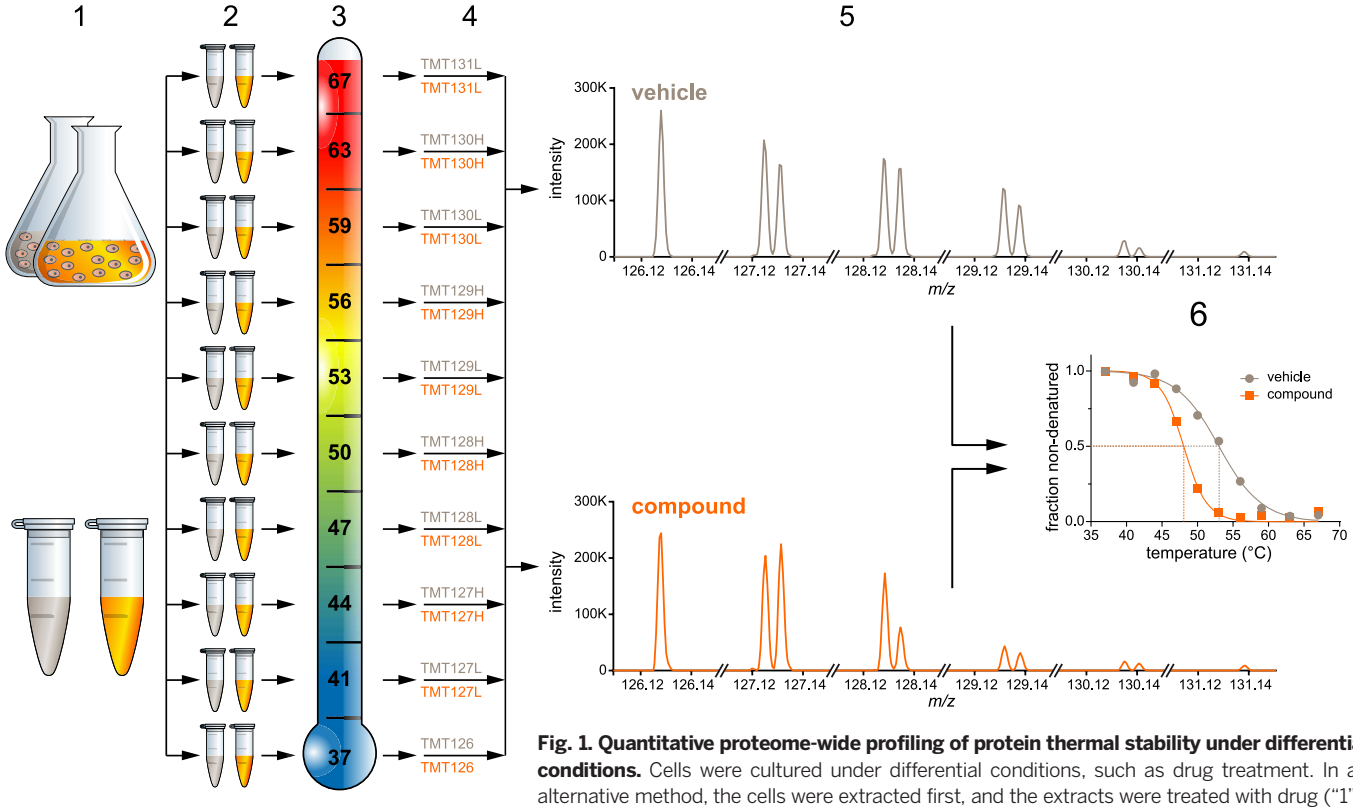

Fig. 1. Quantitative proteome-wide profiling of protein thermal stability under differential conditions. Cells were cultured under differential conditions, such as drug treatment. In an alternative method, the cells were extracted first, and the extracts were treated with drug ("1"). For each condition, the cell or cell-extract sample was divided into 10 aliquots ("2"). Aliquots were subjected to heating at the indicated temperatures. Samples of intact cells were subsequently subjected to extraction with PBS ("3"). After digestion with trypsin, each sample was labeled with a different TMT10 isotope tag ("4"). Subsequently, all samples from each condition were mixed ("4") and analyzed by means of LC-MS/MS ("5"). The obtained reporter ion intensities were used to fit a melting curve and calculate the melting temperature T_m of each protein separately for the two conditions ("6").

of K562 cell extract treated with staurosporine or vehicle were generated as two independent replicates (Fig. 3). Of all proteins, 92% detected yielded curves with sufficiently steep slopes to allow the robust identification of ligand-induced T_m shifts. However, a shallow slope of the melting curve indicated lower melting point reproducibility (Fig. 3A). Whereas most affected proteins showed positive shifts consistent with ligand-induced stabilization, a few proteins, including members of the protein kinase C family, exhibited negative shifts, which may result from destabilization. In total, the thermal profiles comprised 175 protein kinases, of which 51 displayed T_m shifts that passed our significance criteria (Fig. 3B, fig. S6, and table S4). A recent comprehensive analysis of staurosporine targets identified by means of chemoproteomics "kinobeads" profiling (*22*) detected 229 kinases, of which 92 were also present in both biological replicates of the thermal profiles experiments. The limited degree of overlap may be due to the fact that kinobeads will fail to identify kinases that do not bind to the immobilized ligands, whereas thermal profiling will miss proteins owing to insufficient abundance and/or solubility or the absence of a significant ligand effect. Analysis of the 92 kinases common to both data sets revealed that kinobeads identified 66 kinases with a staurosporine median inhibitory concentration (IC_{50}) below 10 μM, of which 34 showed a significant T_m shift, and an additional 15 showed a reproducible shift of greater than 1°C, which could become significant with additional replicates. For some proteins, we observed shallow or irregular curves (for example, BMP2K, AAK1 in fig. S6, G and J, respectively) that may reflect multiple transitions possibly because of independent folding domains and are difficult to fit with our current methods. For the remainder of 17 kinases identified as targets by kinobeads, we observed very small (<1°C) or no T_m shifts (Fig. 3C). These targets may represent false negatives. We also observed thermal shifts for proteins other than kinases. Staurosporine induced apparent stabilization of coproporphyrinogen-III oxidase and ferrochelatase (FECH), two out of the eight enzymes in the heme biosynthesis pathway, for all of which melting curves were obtained (Fig. 3D and fig. S7). Ligand-binding also affected the thermal stability of the regulatory components of some protein complexes—for instance, kinase complexes containing cyclins (fig. S6, C and J). We further explored this in the context of the protein kinase A (PKA) complex (*23*). Inhibition by staurosporine appeared to stabilize the catalytic subunit but destabilize the regulatory subunit. In contrast, the addition of adenosine 3′,5′-monophosphate (cAMP), which causes dissociation of the regulatory subunit from the catalytic subunit, appeared to stabilize the regulatory subunit but destabilize the catalytic subunit, presumably because of the release of the regulatory subunit (Fig. 3E).

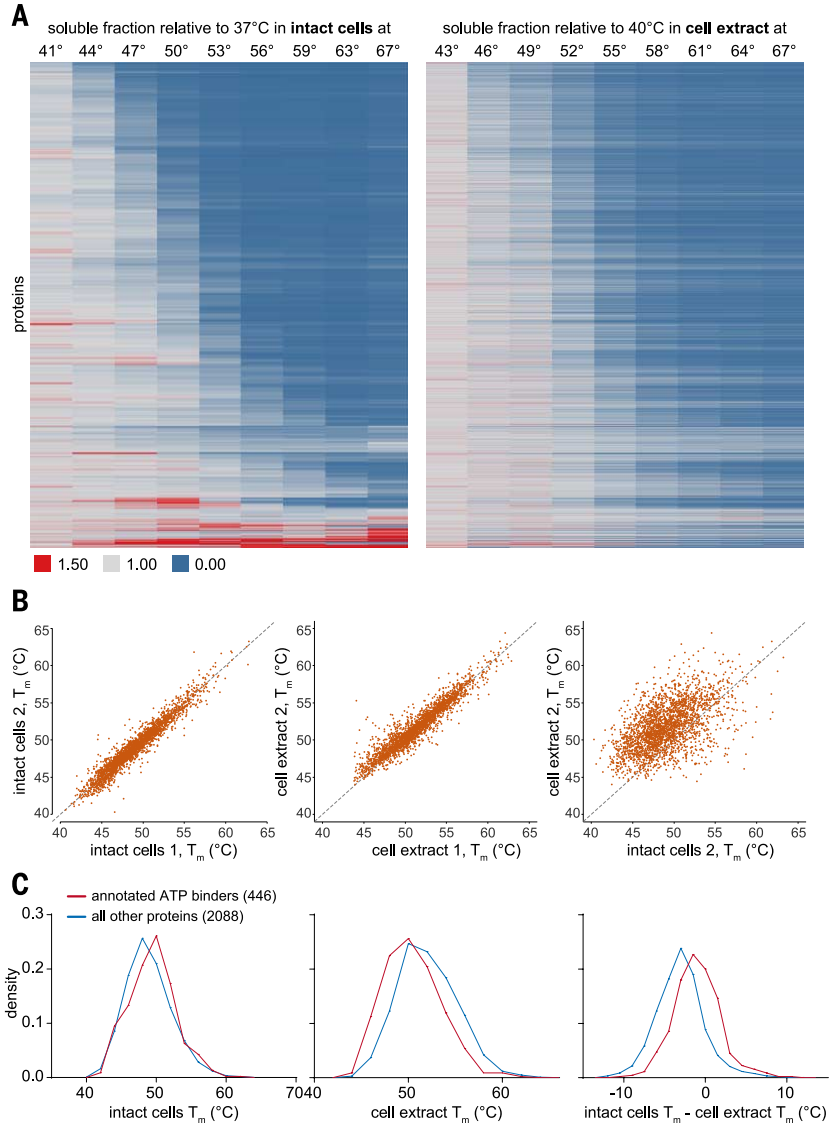

Fig. 2. The thermal proteome profile of a human K562 cell. (**A**) Heat map representation of the thermal stability of 3204 soluble proteins in intact cells (left) and cell extract (right). For each protein, its relative concentration (fold-change) at the indicated temperature compared with the lowest temperature (37°C for intact cells and 40°C for the cell extract) is shown. Protein fold-changes from the experiment on intact cells were clustered. To allow better comparison, proteins heated in the cell extract were plotted in the same order as the proteins heated in intact cells. (**B**) Reproducibility of thermal proteome profiles assessed with replicate experiments on intact cells, R^2 = 0.93 (left), cell extract, R^2 = 0.89 (middle), and direct comparison of proteomes from intact cells and cell-extract experiments, R^2 = 0.30 (right). Most proteins showed greater thermal stability (higher T_m values) in cell extract as compared with intact cells. (**C**) ATP-binding proteins show a trend toward increased stability in intact cells as compared with cell extract. The plots show density distributions of protein T_m values determined in intact cells or in cell extract, and the density distribution of the difference between both settings. A set of 440 proteins annotated as ATP binders show a trend toward increased stability in intact cells. The difference in the means of the distributions was significant (P < 0.01, t test).

Comparison of staurosporine T_m shift data with kinobeads-derived potencies for multiple targets (Fig. 3C) showed no significant correlation between the affinity for staurosporine and the magnitude of the T_m shift. This is not surprising because the extent of thermal stabilization by ligands with a similar binding mode likely depends on the stability of the unliganded protein. To investigate the correlation between ligand affinity and apparent thermal stabilization, we considered a structurally divergent promiscuous kinase inhibitor, GSK3182571 (Fig. 4 and table S5). We identified 13 targets common to both inhibitors with an affinity below 1 μM and a less than 10-fold difference in affinity. For these targets, both compounds showed similar T_m shifts (R^2 = 0.9) (Fig. 4A), suggesting that for a given protein, the T_m shift at saturating ligand concentrations is dependent on the intrinsic affinity of the ligand.

Depending on the number of replicate experiments, ligand-induced T_m shifts as small as 1°C can be monitored. However, to resolve small

changes in ligand-induced thermostability and to enable the ranking of binding affinities among multiple targets, we tailored the isothermal dose-response (ITDR) protocol to a defined set of proteins (*12*). In contrast to the full temperature profiles in which a compound is assayed at a single, typically saturating concentration across 10 temperatures, an ITDR profile is generated at a defined temperature, over a range of compound concentrations. To generate affinity data for GSK3182571, we acquired ITDR profiles (table S6), which showed excellent reproducibility (fig. S8) and were in good agreement with data from kinobeads competition-binding experiments, both for proteins stabilized and proteins destabilized by ligand binding (Fig. 4B and table S7).

Because of its unbiased nature, thermal proteome profiling can detect unexpected off-targets of drug compounds. The heme biosynthesis pathway has not been related to adverse drug effects but is linked to a number of genetic disorders, including erythropoietic protoporphyria, which is caused by a deficiency in FECH and results in high tissue levels of protoporphyrins (*24*). We found two enzymes in the heme pathway interacting with staurosporine and thus asked whether drug interactions with this pathway might result in adverse effects such as skin or liver disease (*25*). The melanoma drug vemurafenib frequently causes severe photosensitivity concomitant with increased levels of protoporphyrins (*26*). ITDR profiling of cells treated with vemurafenib showed that the main proteins affected were its known target BRAF [negative logarithm of the median effective concentration (pEC_{50}) = 6.1] and FECH (pEC_{50} = 5.3) (Fig. 5A and table S8). These concentrations are below the typical steady-state exposure for this drug (*27*) and indicate a less than 10-fold window of target occupancy between the drug's efficacy target and FECH. Alectinib, a second-generation anaplastic lymphoma kinase (ALK) inhibitor for the treatment of non–small-cell lung cancer, was also reported to cause photosensitivity, in contrast to the first-generation drug crizotinib (*28*, *29*). ITDR profiling revealed that alectinib more potently affected FECH than did vemurafenib, whereas crizotinib had no effect (Fig. 5B). These results strongly suggest that the

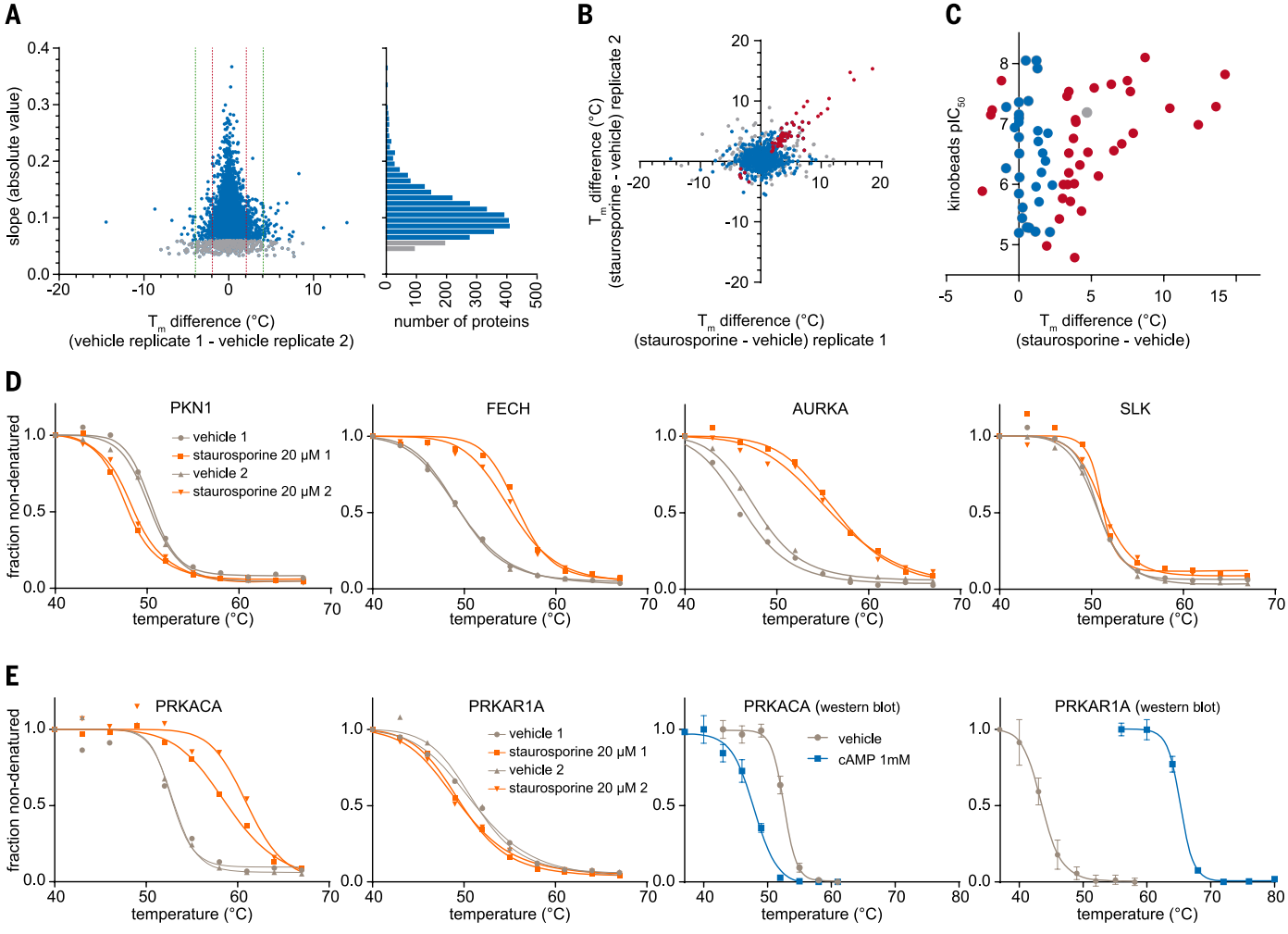

Fig. 3. Differential profiling of drug effects on the thermal proteome profile. Staurosporine treatment of cell extract yields reproducible thermal shifts, allowing robust target identification. (**A**) Cell extract was treated with vehicle or staurosporine. Both experiments were performed as two fully independent replicates. A flat slope of the melting curve relates to lower melting point reproducibility. Melting point differences from the two vehicle experiments are plotted against the shallowest melting curve slope observed in the four vehicle/staurosporine data sets. Proteins with an absolute slope below 0.06 are plotted in gray. The histogram shows the distribution of proteins versus slope values. Of all proteins, 92% yielded curves with sufficiently large slopes. (**B**) Scatter plot of T_m shifts calculated from the two replicates of the staurosporine versus vehicle treatment experiment. Staurosporine-induced T_m shifts that passed the significance criteria are shown in red. Proteins with flat slopes—as shown in gray in (A)—are again shown in gray. (**C**) Comparison between T_m shifts and pIC_{50} values for staurosporine as reported from kinobeads data (*22*). (**D**) Examples of melting curves for PKN1, FECH, AURKA, and SLK with and without staurosporine treatment. (**E**) The catalytic subunit of PKA is stabilized by staurosporine, whereas the regulatory subunit is destabilized. Addition of cAMP followed by Western blot detection revealed destabilization of the catalytic subunit and stabilization of the regulatory subunit. Error bars indicate the SEM from $n = 4$ experiments.

photosensitivity induced by these drugs is mediated by FECH and demonstrates that thermal proteome profiling can serve as a stand-alone technique for obtaining quantitative affinity data for target-ligand interactions in a cell-based setting.

Drug treatment induces T_m shifts for downstream effector proteins

Any modification of a protein can in principle affect its thermal stability. Therefore, comparison of T_m shifts in cell extract, where ligand binding but no downstream effects occur, with T_m shifts in intact cells, where active signaling takes place, might reveal effector proteins downstream of the target. As a model system, we used K562 cells, which are transformed by an oncogenic fusion protein, the BCR-ABL kinase (*30*). Overall, the samples from intact cells yielded a similar protein coverage as that of samples from cell extracts (tables S9 and S10). Cultured cells were treated with vehicle or with the ABL inhibitor dasatinib, a marketed drug against chronic myelogenous leukemia (CML) (*31*) at two concentrations, 0.5 and 5 μM, and the samples were profiled (Fig. 6A and table S9). The minimum T_m shift for each protein was calculated from a pair of replicate experiments. Four proteins displayed significant melting point differences in both the 0.5 and 5 μM dasatinib–treated cell samples. We did not observe a T_m shift for the direct target BCR-ABL, suggesting that this protein is not stabilized by dasatinib binding. However, substantial and significant T_m shifts were observed for the adaptor protein CRKL and the phosphatase SHIP2 (Fig. 6B and fig. S9), which is also known as INPPL1. These proteins are not likely binding the drug directly, and consistent with this, no T_m shift was observed for either protein in cell extracts (table S10). In addition, the BCR-ABL–interacting protein CRK showed a pronounced change in melting curve slope in the dasatinib-treated cells (fig. S9). CRK and CRKL are members of a proto-oncogene family that bind to tyrosine-phosphorylated proteins and are known downstream effectors of BCR-ABL signaling (*32*). CRKL has been previously proposed as a treatment response biomarker (*33*). Comparison of the CRKL melting curves in K562 cells with those in Jurkat cells (table S11), which are not transformed by tyrosine kinase signaling, revealed that dasatinib treatment of K562 cells reverted the thermal stability of CRKL to the level observed in Jurkat cells (Fig. 6C), and the same effect was observed for CRK (fig. S10). The Jurkat cell profiles also revealed that ABL1 kinase appeared to be more thermostable compared with the BCR-ABL fusion protein in K562 cells, suggesting that thermal profiling could be used to identify protein fusions which are difficult to identify by expression proteomics (Fig. 6C). In order to evaluate the drug concentration dependence of the T_m-shifted effector proteins, we performed ITDR profiles at three different temperatures (Fig. 6D, fig. S11, and table S12). The concentrations eliciting half-maximal response of the CRKL marker in the ITDR profiles recorded at three different temperatures were between 1.5 and 3.2 nM, which is in good agreement with the known potency of dasatinib for the inhibition of cell growth (*34*). In-depth analysis of the 50°C ITDR data revealed additional markers that either showed small T_m shifts or, in the case of the known downstream effector CRK, a pronounced change in the melting curve slope, indicating that the ITDR profiles can offer greater sensitivity than the full-temperature profiles (fig. S11). It is tempting to speculate that the most sensitive biomarkers are those that exhibit large or even stoichiometric changes in protein state, which should be robustly detected by their T_m shift. This contrasts with the use of a

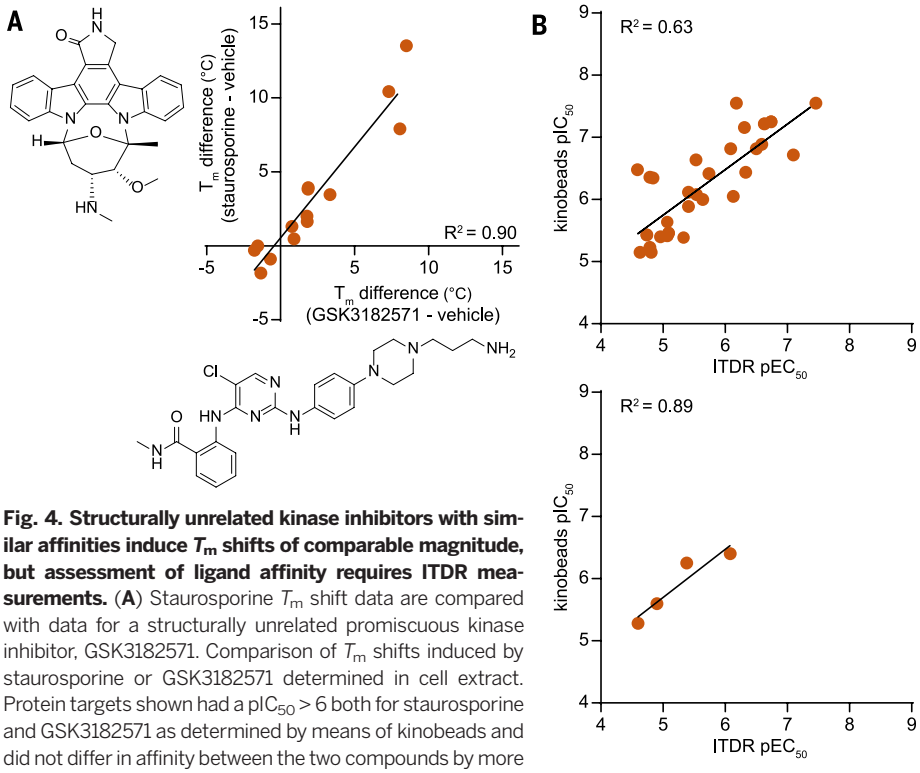

Fig. 4. Structurally unrelated kinase inhibitors with similar affinities induce T_m shifts of comparable magnitude, but assessment of ligand affinity requires ITDR measurements. (**A**) Staurosporine T_m shift data are compared with data for a structurally unrelated promiscuous kinase inhibitor, GSK3182571. Comparison of T_m shifts induced by staurosporine or GSK3182571 determined in cell extract. Protein targets shown had a $pIC_{50} > 6$ both for staurosporine and GSK3182571 as determined by means of kinobeads and did not differ in affinity between the two compounds by more than one order of magnitude. (**B**) Good agreement between GSK3182571 pEC_{50} values determined by means of ITDR, with pIC_{50} values determined with kinobeads. (Top) Proteins stabilized by GSK3182571 treatment. (Bottom) Proteins destabilized by GSK3182571 treatment.

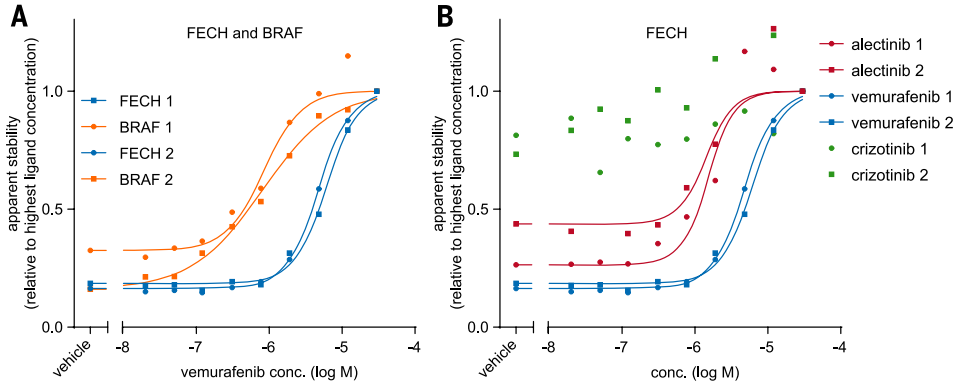

Fig. 5. The clinical kinase drugs vemurafenib and alectinib, which can cause phototoxicity as a side effect, induce T_m shifts in the heme biosynthesis enzyme FECH. (**A**) Concentration-dependent target occupancy of vemurafenib and its cognate target BRAF compared with the off-target FECH. ITDR profiling was performed at 55°C with vemurafenib-treated K562 cells and showed concentration-dependent thermal stabilization of FECH and BRAF. The data are normalized so that the quantity of soluble target at the highest compound concentration, which reflects maximum thermal stabilization, is set to 1 and fixed for curve-fitting. (**B**) ITDR performed at 55°C with K562 cells treated with vemurafenib, alectinib, or crizotinib over a range of concentrations. Alectinib displays a more potent effect on FECH as compared with that by vemurafenib, whereas crizotinib, a drug not known to cause photosensitivity, has no effect.

posttranslational modification as a biomarker where it is usually difficult to assess the stoichiometry of the modification.

In general terms, the thermal stability of a protein may be defined by its mutational status, posttranslational modifications, and bound ligands such as other proteins, cofactors, metabolites, or drugs. Fusion proteins, splice variants, and posttranslational modifications are typically undersampled and therefore not comprehensively detected in MS-based proteomics. Hence, the thermal proteome profile of a human cell can provide a general view of the proteomic state, or proteotype.

The future scope and applicability of thermal proteome profiling will substantially benefit from continued advances in the sensitivity and accuracy of MS-based proteomics. Future developments should include the development of protocols for membrane proteins and the application to tissues from animal studies or clinical biopsies.

Materials and methods

Reagents and cell culture

Reagents and media were purchased from Sigma-Aldrich (St. Louis, MO) unless otherwise noted. PBS was prepared by using 137 mM NaCl, 2.7 mM KCl, 10 mM Na_2HPO_4, and 2 mM KH_2PO_4 to buffer at pH 7.4 and supplemented with complete EDTA-free protease inhibitor cocktail (one tablet per 25 ml) (Roche Diagnostics, Basel Switzerland). Staurosporine was from Calbiochem (Millipore, Billerica, MA), vemurafenib and crizotinib from Selleck (Houston, TX), alectinib from MedchemExpress (Monmouth Junction, NJ), and dasatinib from Toronto Research (Toronto, Canada). The synthesis of GSK3182571 is described in the supplementary methods. DNA fragments PG1 (5′-AGC TTA GAC ATG CCT AGA CAT GCC TA -3′) and PG2 (5′-AGC TTA GGC ATG TCT AGG CAT GTC TA -3′) were from Life Technologies (Carlsbad, CA) and dissolved in 100 mM Tris (pH7.5), 1 mM NaCl and 10m M EDTA. K562, Jurkat E6.1, and A549 cells were from ATCC; K562 and A549 cells were cultured in RPMI medium containing 10% fetal calf serum (FCS) and Jurkat E6.1 cells in RPMI1640 supplemented with 4.5 g/l glucose, 10 mM HEPES, 1 mM sodium pyruvate, and 10% FCS. HT-29 (ATTC no. HTB-38) were maintained in Dulbecco's Modified Eagle Medium. Culture media were supplemented with 0.3 g/L L-glutamine and 10% fetal bovine serum (FBS) (Gibco, Carlsbad, CA), 100 units/mL penicillin, and 100 units/mL streptomycin. The cells were expanded to a maximum of 2×10^6 cells/ml in case of K562 and 10^7 cells/ml in case of Jurkat E6.1.

Preparation of cell extract for CETSA with Western blot read-out

A549 and HT-29 cells were harvested and washed with PBS. The cells were diluted in KB buffer (25 mM Tris-HCl supplemented with 5 mM beta-glycerophosphate, 2 mM DTT, 0.1 mM Na_3VO_4, 10 mM $MgCl_2$, and complete protease inhibitor cocktail). The cell suspensions were freeze-thawed three times by using liquid nitrogen. The soluble fraction was separated from the cell debris by centrifugation at 20,000 g for 20 min at 4°C. For the CETSA melting curve experiments, cell extracts were diluted with KB buffer and divided into two aliquots, with one aliquot being treated with ligand/DNA fragments depending on the target and the other aliquot treated with the solvent of the ligand (control). After 10 min incubation at room temperature, the respective cell extracts were heated individually at different temperatures for 3 min in a thermal cycler [Applied Biosystems (Foster City, CA)/Life Technologies] followed by cooling for 3 min at room temperature. The heated cell extracts were centrifuged at 20,000 g for 20 min at 4°C in order to separate the soluble fractions from precipitates. The supernatants were transferred to new 0.2 mL microtubes and analyzed by means of Western blot analysis. NuPage Bis-Tris 4-12% polyacrylamide gels with MES SDS running buffer (Life Technologies) were used for separation of proteins in the samples. Proteins were transferred to nitrocellulose membranes by using the iBlot system (Life Technologies). Primary antibodies anti-PKA Regulatory I-α (sc-136231), anti-PKA Catalytic-α

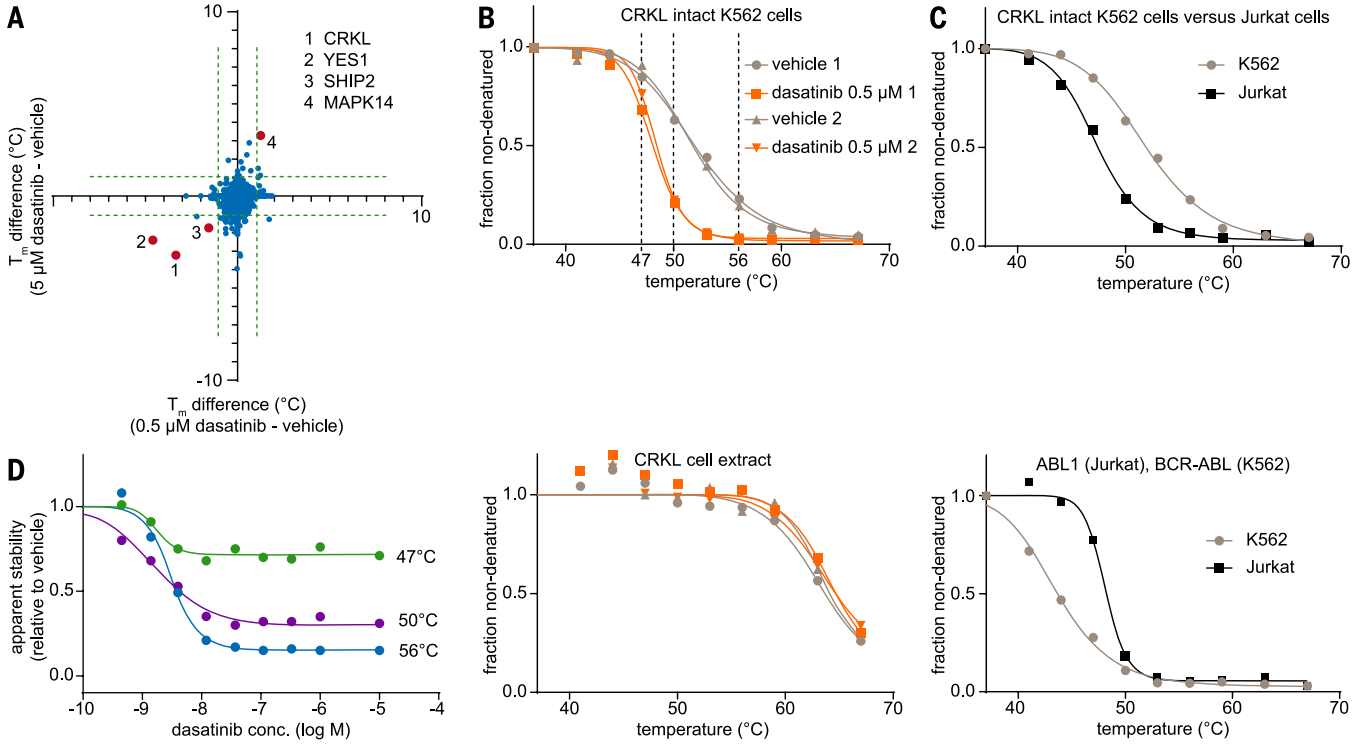

Fig. 6. Treatment of K562 cells with dasatinib induces T_m shifts for downstream effector proteins in the BCR-ABL pathway. (**A**) Cell-wide assessment of T_m shifts induced by dasatinib (0.5 and 5 µM) in K562 cells. The minimum T_m shift for each protein was calculated from a pair of full replicate experiments. Four proteins showing significant melting point differences both in the 0.5 and 5 µM dasatinib data sets are marked in red. (**B**) Effect of dasatinib on the melting curves for the effector protein CRKL, determined in two biological replicates in intact cells (top) and cell extracts (bottom). (**C**) The melting curve for CRKL in Jurkat cells closely matches the curve obtained in dasatinib-treated K562 cells (top). The ABL1 protein in Jurkat cells is much more thermostable compared with the BCR-ABL fusion protein in K562 cells. (**D**) ITDR curves for CRKL in dasatinib-treated intact cells. Experiments were performed at 47°C (green curve), 50°C (purple curve), and 56°C (blue curve).

(sc-28315), anti-p53 WT, and R273H (sc-126); secondary goat anti-mouse HRP-IgG (sc-2055) and bovine anti-goat HRP-IgG (sc-2352) antibodies (Santa Cruz Biotechnology, Dallas, TX) were used for immunoblotting. Chemiluminescence intensities were detected and quantified by using a ChemiDoc XRS+ imaging system with Image Lab software (Bio-Rad, Hercules, CA). Data were expressed as means ± SEM. The data (band intensities) from multiple runs ($n \geq 3$) were plotted with Graphpad Prism software.

Preparation of cell extract for thermal proteome profiling

Suspension cultures of K562 cells (1.5 to 2 × 10^6 cells/ml) or of Jurkat E6.1 cells (4 × 10^6 cells/ml) were centrifuged at 340 g for 2 min at 4°C. The cells were resuspended in 50 ml PBS. After a second centrifugation step as above, the cells were resuspended in 10 ml ice-cold PBS and centrifuged again at 340 g for 2 min at 4°C. The cells were resuspended in 1.5 ml of ice-cold PBS and snap-frozen in liquid nitrogen. The tube was placed into a water bath at 23°C until ~60% of the content was thawed and then transferred on ice until the entire content was thawed. This freeze/thaw cycle was repeated twice before the samples were subjected to ultracentrifugation (20 min at 4°C and 100,000 g). The protein concentration of the supernatant was determined by Bradford assay (Bio-Rad), and aliquots were snap-frozen in liquid nitrogen for use in subsequent thermal shift assays.

Thermal profiling using cell extract

A solution of the compound in dimethyl sulfoxide (DMSO) or DMSO alone as vehicle (Table 1) was added to the cell extract to 1% final DMSO concentration. The extract was then incubated for 10 min at 23°C, divided into 10 aliquots of 100 µl, and transferred into 0.2-ml polymerase chain reaction (PCR) tubes. One each of the compound and of the vehicle containing samples was heated in parallel for 3 min to the respective temperature, followed by a 3-min incubation time at room temperature. Subsequently, the extract was centrifuged at 100,000 g for 20 min at 4°C. The supernatant was fractionated by means of SDS gel electrophoresis and subjected to sample preparation for MS analysis. For ITDR experiments, GSK3182571 was tested as a nine-point serial dilution starting at 100 µM (resulting in concentrations of 100, 33.3, 11.1, 3.70, 1.235, 0.412, 0.137, 0.046, and 0.015 µM), including one vehicle control in an isothermal dose-response experiment at 53°C following the procedure outlined above for experiments in cell extract.

Thermal profiling using intact cells

To 24 ml of a suspension of K562 cells (at a density of 1.5 * 10^6 cells/ml) or Jurkat E6.1cells (at a density of 4 * 10^6 cells/ml) in a T-flask, a volume of either 120 µl of a solution of the reference compound dissolved in DMSO or an equivalent amount of DMSO (vehicle) was added. Incubation of cells with compound and vehicle was conducted in parallel for the duration of 1 hour at 37°C and 5%CO_2. Cells were pelleted at 340 g and 4°C for 2 min, resuspended in 20 ml of ice cold PBS, and centrifuged again as indicated above. This washing step was repeated once, and the cells were carefully resuspended in 1200 µl PBS. 100 µl of this resulting cell suspension was transferred into 0.2-ml PCR tubes and subjected to a centrifugation step at 325 g for 2 min at 4°C. Using a pipette, 80 µl of the PBS supernatant was removed. By gently tapping the tubes, the cells were resuspended, and one each of the compound and of the vehicle containing tubes was heated in parallel in a PCR machine for 3 min to the respective temperature (37°C to 67°C), followed by a 3-min incubation time at room temperature. Thereafter, the cells were snap-frozen in liquid nitrogen for 1 min. The cells were thawed briefly in a water bath at 25°C, transferred on ice, and resuspended by using a pipette. This freeze-thaw cycle was repeated once. After an addition of further 30 µl of PBS and resuspension, the entire content was centrifuged at 100,000 g for 20 min at 4°C. After centrifugation, 30 µl of the supernatant were transferred into a new tube. Protein concentration of the 37°C and 41°C samples were determined and used to normalize loading of SDS gels. Proteins in the supernatant were denatured by using SDS sample buffer, partially separated by means of SDS gel electrophoresis, and subjected to sample preparation for MS analysis. For ITDR experiments, vemurafenib, alectinib, and crizotinib were used as a nine-point serial dilution starting at 30 µM (concentrations were 30, 12, 4.8, 1.92, 0.77, 0.31, 0.12, 0.05, and 0.02 µM), including one vehicle control at 55°C following the procedure outlined above. Dasatinib was tested as an eight-point serial dilution starting at 1 µM (concentrations used were 1, 0.33, 0.111, 0.037, 0.012, 0.004, 0.0013, and 0.00046 µM), including one dasatinib control at 10 µM and one vehicle control on intact cells at 47°C, 50°C, and 56°C following the procedure outlined above for experiments on intact cells (Table 1).

Table 1. Compounds used in thermal profiling. Dashes indicate that compound was not tested in intact cells.

Compound	Concentration used in cellular extract experiments	Concentration(s) in intact cell experiments	Cell line
MgATP	2 mM	—	K562
staurosporine	20 µM	—	K562
cAMP	1 mM	—	K562
GSK3182571	20 µM	—	K562
dasatinib	5 µM	0.5 µM, 5 µM	K562
p53 WT			
PG1	100 µM	—	A549
PG2	100 µM	—	A549
p53 R273H			
PG1	100 µM	—	HT-29
PG2	100 µM	—	HT-29

Kinobeads assays

Competition binding assays were performed as described previously by using a modified bead matrix (*5*, *22*). Briefly, 1 ml (5 mg protein) cell extract was pre-incubated with test compound or vehicle for 45 min at 4°C followed by incubation with kinobeads (35 µl beads per sample) for 1 hour at 4°C. The beads were washed with lysis buffer and eluted with 50 µl 2× SDS sample buffer. GSK3182571 was tested at 10, 2.5, 0.625, 0.15625, 0.03906, 0.00977, and 0.00244 µM.

Sample preparation for MS

Gel lanes were cut into three slices covering the entire separation range (~2 cm) and subjected to in-gel digestion (*5*). Peptide samples were labeled with 10-plex TMT (TMT10, Thermo Fisher Scientific, Waltham, MA) reagents, enabling relative quantification of a broad range of 10 temperature points in a single experiment (*15*, *22*). For kinobeads and ITDR experiments, either 10 or 8 TMT labels were used depending on the compound concentration range chosen. The labeling reaction was performed in 40 mM triethylammoniumbicarbonate, pH 8.53 at 22°C and quenched with glycine. Labeled peptide extracts were combined to a single sample per experiment, and as indicated in the supplementary materials, for most samples additional fractionation was performed by using reversed-phase chromatography at pH 12 [1 mm Xbridge column (Waters, Milford, MA)], as previously described (table S13) (*35*).

LC-MS/MS analysis

Samples were dried in vacuo and resuspended in 0.05% trifluoroacetic acid in water. Of the sample, 50% was injected into an Ultimate3000 nanoRLSC (Dionex, Sunnyvale, CA) coupled to a Q Exactive (Thermo Fisher Scientific). Peptides were separated on custom 50 cm × 100 µM (ID) reversed-phase columns (Reprosil) at 40°C. Gradient elution was performed from 2% acetonitrile to 40% acetonitrile in 0.1% formic acid over 2 hours. Samples were online injected into Q-Exactive mass spectrometers operating with a data-dependent top 10 method. MS spectra were acquired by using 70.000 resolution and an ion target of 3E6. Higher energy collisional dissociation (HCD) scans were performed with 35% NCE at 35.000 resolution (at m/z 200), and the ion target settings was set to 2E5 so as to avoid coalescence (*15*). The

instruments were operated with Tune 2.2 or 2.3 and Xcalibur 2.7 or 3.0.63.

Peptide and protein identification

Mascot 2.4 (Matrix Science, Boston, MA) was used for protein identification by using a 10 parts per million mass tolerance for peptide precursors and 20 mD (HCD) mass tolerance for fragment ions. Carbamidomethylation of cysteine residues and TMT modification of lysine residues were set as fixed modifications and methionine oxidation, and N-terminal acetylation of proteins and TMT modification of peptide N-termini were set as variable modifications. The search database consisted of a customized version of the International Protein Index protein sequence database combined with a decoy version of this database created by using a script supplied by Matrix Science. Unless stated otherwise, we accepted protein identifications as follows: (i) For single-spectrum to sequence assignments, we required this assignment to be the best match and a minimum Mascot score of 31 and a 10× difference of this assignment over the next best assignment. Based on these criteria, the decoy search results indicated <1% false discovery rate (FDR). (ii) For multiple spectrum to sequence assignments and using the same parameters, the decoy search results indicate <0.1% FDR. All identified proteins were quantified; FDR for quantified proteins was <1%.

Peptide and protein quantification

Reporter ion intensities were read from raw data and multiplied with ion accumulation times (the unit is milliseconds) so as to yield a measure proportional to the number of ions; this measure is referred to as ion area (*36*). Spectra matching to peptides were filtered according to the following criteria: mascot ion score >15, signal-to-background of the precursor ion >4, and signal-to-interference >0.5 (*37*). Fold-changes were corrected for isotope purity as described and adjusted for interference caused by co-eluting nearly isobaric peaks as estimated by the signal-to-interference measure (*38*). Protein quantification was derived from individual spectra matching to distinct peptides by using a sum-based bootstrap algorithm; 95% confidence intervals were calculated for all protein fold-changes that were quantified with more than three spectra (*36*).

Curve fitting, normalization, and estimation of slope and melting point differences for CETSA experiments

Melting curves

For all CETSA experiments, fold-changes were calculated by using the lowest temperature condition as the reference. Relative fold changes as a function of temperature followed a sigmoidal trend, which was fitted with the following equation derived from chemical denaturation theory (*39*) (en.wikipedia.org/wiki/Equilibrium_unfolding) using R (www.r-project.org):

$$f(T) = \frac{1 - plateau}{1 + e^{-\left(\frac{a}{T} - b\right)}} + plateau$$

Where T is the temperature and a, b, and $plateau$ are constants. The value of $f(T)$ at the lowest temperature T_{min} was fixed to one. The melting point of a protein is defined as the temperature T_m at which half of the protein amount has been denatured:

$$f(T_m) = 0.5$$

Additionally, the slope of the melting curve is defined as the value of the first derivative of $f(T)$ at the point $T = T_{infl}$:

$$\text{slope} = f'(T_{infl})$$

where T_{infl} is the inflection point of the curve, meaning that the second derivative of $f(T)$ equals zero at $T = T_{infl}$:

$$f''(T_{infl}) = 0$$

Normalization

The vehicle and compound-treated experiments were normalized in the following way:

Selection of proteins for normalization: (i) The set of proteins, identified in both experiments termed "jointP" was determined. (ii) For each experiment (vehicle or compound) all proteins from jointP fulfilling the following criteria were collected: the fold-changes at the seventh highest temperature point compared with the lowest temperature point were between 0.4 and 0.6, and at the 9th and 10th highest temperature points compared th the lowest temperature point were below 0.3 and 0.2 respectively. (iii) The bigger of these two protein subsets was then used for normalization (typically more than 200 proteins qualified). This protein set is referred to as "normP."

Calculation of correction factors: (i) The median fold-change values over all proteins in normP were calculated for each of the 10 fold-changes. This was done separately for both experiments, and for each experiment a melting curve was fitted. The curve that was fitted with the best R^2 was used to normalize both experiments. (ii) For each experiment, the correction factors were calculated by using the median fold-changes of the proteins in normP. For each median fold-change, a correction factor by which that fold-change would have to be multiplied with in order to coincide with the best-fitting curve was calculated.

Normalization: The two sets of correction factors were applied to all the protein fold-changes in the respective experiments.

This heuristic normalization procedure covers three important aspects. (i) The same subset of proteins is used to determine normalization coefficients in both experiments, thus circumventing any potential bias caused by proteins only identified in one experiment. (ii) The subselection of late-melting proteins (seventh point between 0.4 and 0.6) ensures that the normalization of high-temperature points will be more accurate. (iii) Last, the narrow requirements on the 7th, 9th, and 10th points will ensure that a narrow range of melting profiles is used for calculating the points from which the normalization curve will be derived. This is important because if vastly different melting profiles are combined into a single one, the above equation will not necessarily fit well. A normalization curve example as well as melting curves of several proteins before and after normalization are illustrated in fig. S12.

Estimation of slope and melting point differences

After normalization, melting curves were fitted for all proteins identified in the vehicle- and compound-treated experiments. Melting point differences and slope differences were calculated for proteins whose curves passed the following two requirements: (i) both fitted curves for the vehicle and compound treated condition had an R^2 of greater than 0.8, and (ii) the vehicle curve had a *plateau* of less than 0.3.

Typically close to 80% of proteins that were identified in both the vehicle- and compound-treated experiment passed these criteria. The slope of the curves had the biggest impact on the reproducibility of melting point differences of proteins. This observation can be rationalized in the following way. If the curve has a shallow slope, then small changes with respect to the reference point—in our case, the lowest temperature—will have a strong impact on where the curve crosses the 0.5 fold-change level (melting point). Consequently, small variations in the quantitative measurement of the MS signals corresponding to the lowest temperature will lead to strong shifts in the inferred melting point of the curve. This means that it is difficult to get high precision measurements of melting point differences when comparing two curves with shallow slopes. If the curve, however, has a steep slope then the melting point measurement will not be substantially affected by small variations of the quantitative measurements of the lowest temperature, nor of any other temperature points. Taking this into account, we used the following strategy for significance estimation of protein melting point differences between vehicle- and compound-treated experiments, which is conceptually very similar to a broadly used strategy for inferring significant protein fold-changes (*40*). The calculated melting point differences of proteins were ordered in descending slope order (those with the shallowest slope come first), in which the slope for each protein is the lowest (steepest) slope calculated from the two curve fits performed for the protein in the vehicle- and compound-treated condition. The proteins were divided into bins. The bins are constructed starting from proteins with the highest (shallowest) slope. Each bin consists of at least 300 proteins. Once each bin has been completed, the remaining number of proteins is counted; if this number is below 300, the remaining proteins are added to the last completed bin. This data quality–dependent binning strategy is analogous to the procedure described in Cox *et al.* with the only difference being that proteins are sorted by slope instead of abundance (*40*). The statistical significance of differences in protein melting points was calculated by estimating the left- and right-sided robust standard deviation of the distribution of the measurements using the 15.87, 50, and 84.13 percentiles and calculating the P values for all measurements for a specific bin exactly as previously described (*40*). Subsequently,

an adjustment for multiple hypothesis testing was performed on the full data set by using Benjamini-Hochberg (BH) correction (*41*).

In order to select proteins whose thermal stability is significantly changed by compound treatment in two biological replicates (two pairs of vehicle- and compound-treated experiments) the following rules were used: (i) The melting point difference between vehicle- and compound-treated conditions for a protein had a BH-corrected P value of less than 0.05 in one biological replicate and less than 0.10 in the other. (ii) Both melting point differences were either positive or negative in the two biological replicates. (iii) The smallest absolute melting point difference of the protein in the two biological replicates was greater than the absolute melting point difference of that same protein between the two vehicle experiments. (iv) In each biological replicate, the steepest slope of the protein melting curve in the vehicle- and compound-treated conditions pair was below –0.06.

Given the stringent requirements on the quality of the curve fits of the compared proteins, we allowed proteins quantified with single peptides to be part of the analysis.

Calculation of pEC_{50} values from ITDR experiments

For isothermal dose-response experiments, the vehicle condition was used as the reference for fold-change calculation. For proteins stabilized by the compound treatment, at least a 50% increase in protein stabilization at the highest compound concentration compared with the vehicle condition ($FC_{\text{highest concentration}}$ >1.5) was required in order to attempt to calculate a pEC_{50}. Before fitting the sigmoidal dose response curve (fitted by using GraphPad Prism, top and bottom fixed at 1 and 0 respectively, variable slope), all fold-change values were transformed as follows:

$$FC_{\text{transformed}} = (FC - 1)/(FC_{\text{highest concentration}} - 1)$$

After this transformation, the fold-change value is zero at the vehicle condition and one at the condition corresponding to the highest drug concentration. In order to ascertain that the protein stabilization was due to compound treatment and not random fluctuations, we additionally required that the fitted sigmoidal curve had an R^2 of at least 0.8. Because the transformed fold-change at the highest compound concentration condition was fixed at one, this concentration was assumed to be sufficiently high to achieve the maximum effect of the compound-induced protein stabilization.

For proteins destabilized by the compound treatment, at least a 50% increase in protein stabilization at the vehicle condition compared with the condition with the highest compound concentration was required ($FC_{\text{highest concentration}}$ < 0.6666). In this case, the fold-changes were transformed as follows:

$$FC_{\text{transformed}} = (FC - FC_{\text{highest concentration}})/(1 - FC_{\text{highest concentration}})$$

After this transformation, the fold-change value is 1 at the vehicle condition, and 0 at the condition corresponding to the highest drug concentration. The sigmoidal curve fits and $R^2 > 0.8$ criterion were performed and applied in the same way as above. Conversely, here it has to be assumed that the transformed fold-change at the highest compound concentration is sufficiently high in order for the compound-induced protein destabilization to have reached the maximum effect. Given the potentially narrow fold-change range, we required proteins to be quantified with more than three spectra in order to consider them for pEC_{50} calculations.

pIC_{50} calculations

For kinobeads experiments, the vehicle condition was used as the reference for fold-change calculation. Sigmoidal dose-response curves were fitted by using R (www.r-project.org) and the drc package (www.bioassay.dk) as previously described (*5*).

Heat map generation

Only proteins that were quantified with at least two distinct peptides in the intact-cell experiment and additionally were quantified in the second intact-cell experiment and in the two cell-extract experiments were included (table S1). The clustering was performed in Spotfire by using complete linkage with Euclidean distance.

GO analysis

The web tool Gorilla (cbl-gorilla.cs.technion.ac.il) (*42*) was used to identify enriched GO terms in (i) selected clusters in the melting proteome heatmap (Fig. 2 and fig. S2) by using all the proteins in the whole-cell heatmap as background and (ii) the 200 proteins with the highest or lowest melting temperature in the whole-cells experiment and the cell extract as well as for the 200 proteins with the biggest positive or negative difference between whole cells and cell extract. For the second enrichment analysis, all proteins that were present in both the whole-cell experiment and the cell-extract experiment and fulfilled the filtering criteria described above were used as background. Significant (FDR Q value < 0.01) GO terms are reported in table S2.

REFERENCES AND NOTES

1. M. Wilhelm *et al*., Mass-spectrometry-based draft of the human proteome. *Nature* **509**, 582–587 (2014). doi: 10.1038/nature13319; pmid: 24870543
2. N. A. Kulak, G. Pichler, I. Paron, N. Nagaraj, M. Mann, Minimal, encapsulated proteomic-sample processing applied to copy-number estimation in eukaryotic cells. *Nat. Methods* **11**, 319–324 (2014). doi: 10.1038/nmeth.2834; pmid: 24487582
3. J. Cox, M. Mann, Quantitative, high-resolution proteomics for data-driven systems biology. *Annu. Rev. Biochem.* **80**, 273–299 (2011). doi: 10.1146/annurev-biochem-061308-093216; pmid: 21548781
4. A. Bensimon, A. J. Heck, R. Aebersold, Mass spectrometry-based proteomics and network biology. *Annu. Rev. Biochem.* **81**, 379–405 (2012). doi: 10.1146/annurev-biochem-072909-100424; pmid: 22439968
5. M. Bantscheff *et al*., Quantitative chemical proteomics reveals mechanisms of action of clinical ABL kinase inhibitors. *Nat. Biotechnol.* **25**, 1035–1044 (2007). doi: 10.1038/nbt1328; pmid: 17721511
6. M. Bantscheff *et al*., Chemoproteomics profiling of HDAC inhibitors reveals selective targeting of HDAC complexes. *Nat. Biotechnol.* **29**, 255–265 (2011). doi: 10.1038/nbt.1759; pmid: 21258344
7. A. P. Frei *et al*., Direct identification of ligand-receptor interactions on living cells and tissues. *Nat. Biotechnol.* **30**, 997–1001 (2012). doi: 10.1038/nbt.2354; pmid: 22983091
8. G. E. Winter *et al*., Systems-pharmacology dissection of a drug synergy in imatinib-resistant CML. *Nat. Chem. Biol.* **8**, 905–912 (2012). doi: 10.1038/nchembio.1085; pmid: 23023260
9. J. S. Duncan *et al*., Dynamic reprogramming of the kinome in response to targeted MEK inhibition in triple-negative breast cancer. *Cell* **149**, 307–321 (2012). doi: 10.1016/j.cell.2012.02.053; pmid: 22500798
10. C. N. Pace, T. McGrath, Substrate stabilization of lysozyme to thermal and guanidine hydrochloride denaturation. *J. Biol. Chem.* **255**, 3862–3865 (1980). pmid: 7372654
11. M. Vedadi *et al*., Chemical screening methods to identify ligands that promote protein stability, protein crystallization, and structure determination. *Proc. Natl. Acad. Sci. U.S.A.* **103**, 15835–15840 (2006). doi: 10.1073/pnas.0605224103; pmid: 17035505
12. D. Martinez Molina *et al*., Monitoring drug target engagement in cells and tissues using the cellular thermal shift assay. *Science* **341**, 84–87 (2013). doi: 10.1126/science.1233606; pmid: 23828940
13. G. M. Simon, M. J. Niphakis, B. F. Cravatt, Determining target engagement in living systems. *Nat. Chem. Biol.* **9**, 200–205 (2013). doi: 10.1038/nchembio.1211; pmid: 23508173
14. J. A. Fraser *et al*., A novel p53 phosphorylation site within the MDM2 ubiquitination signal: II. A model in which phosphorylation at SER269 induces a mutant conformation to p53. *J. Biol. Chem.* **285**, 37773–37786 (2010). doi: 10.1074/jbc.M110.143107; pmid: 20847049
15. T. Werner *et al*., Ion coalescence of neutron encoded TMT 10-plex reporter ions. *Anal. Chem.* **86**, 3594–3601 (2014). doi: 10.1021/ac500140s; pmid: 24579773
16. B. I. Kurganov, Kinetics of protein aggregation. Quantitative estimation of the chaperone-like activity in test-systems based on suppression of protein aggregation. *Biochemistry (Mosc.)* **67**, 409–422 (2002). doi: 10.1023/A:1015277805345; pmid: 11996654
17. I. Asial *et al*., Engineering protein thermostability using a generic activity-independent biophysical screen inside the cell. *Nat. Commun.* **4**, 2901 (2013). doi: 10.1038/ncomms3901; pmid: 24352381
18. S. Ebbinghaus, A. Dhar, J. D. McDonald, M. Gruebele, Protein folding stability and dynamics imaged in a living cell. *Nat. Methods* **7**, 319–323 (2010). doi: 10.1038/nmeth.1435; pmid: 20190760
19. I. Becher *et al*., Affinity profiling of the cellular kinome for the nucleotide cofactors ATP, ADP, and GTP. *ACS Chem. Biol.* **8**, 599–607 (2013). doi: 10.1021/cb3005879; pmid: 23215245
20. W. S. El-Deiry, S. E. Kern, J. A. Pietenpol, K. W. Kinzler, B. Vogelstein, Definition of a consensus binding site for p53. *Nat. Genet.* **1**, 45–49 (1992). doi: 10.1038/ng0492-45; pmid: 1301998
21. L. Zhang *et al*., Characterization of the novel broad-spectrum kinase inhibitor CTx-0294885 as an affinity reagent for mass spectrometry-based kinome profiling. *J. Proteome Res.* **12**, 3104–3116 (2013). doi: 10.1021/pr3008495; pmid: 23692254
22. T. Werner *et al*., High-resolution enabled TMT 8-plexing. *Anal. Chem.* **84**, 7188–7194 (2012). doi: 10.1021/ac301553x; pmid: 22881393
23. P. Zhang *et al*., Structure and allostery of the PKA RIIβ tetrameric holoenzyme. *Science* **335**, 712–716 (2012). doi: 10.1126/science.1213979; pmid: 22323819
24. H. A. Dailey, P. N. Meissner, Erythroid heme biosynthesis and its disorders. *Cold Spring Harb. Perspect. Med.* **3**, a011676 (2013). doi: 10.1101/cshperspect.a011676; pmid: 23471474
25. S. Wahlin, P. Harper, Skin ferrochelatase and photosensitivity in mice and man. *J. Invest. Dermatol.* **130**, 631–633 (2010). doi: 10.1038/jid.2009.246; pmid: 19657351
26. P. Gelot *et al*., Vemurafenib: An unusual UVA-induced photosensitivity. *Exp. Dermatol.* **22**, 297–298 (2013). doi: 10.1111/exd.12119; pmid: 23528218
27. G. Bollag *et al*., Clinical efficacy of a RAF inhibitor needs broad target blockade in BRAF-mutant melanoma. *Nature* **467**, 596–599 (2010). doi: 10.1038/nature09454; pmid: 20823850
28. C. A. Perez, M. Velez, L. E. Raez, E. S. Santos, Overcoming the resistance to crizotinib in patients with non-small cell lung cancer harboring EML4/ALK translocation. *Lung Cancer* **84**, 110–115 (2014). doi: 10.1016/j.lungcan.2014.02.001; pmid: 24598368
29. S. Ou *et al*., paper presented at the European Cancer Congress 2013, abstract 44 (2013); available at http://eccamsterdam2013.ecco-org.eu/Scientific-Programme/Abstract-search.aspx?abstractid=8959.

30. Y. Ben-Neriah, G. Q. Daley, A. M. Mes-Masson, O. N. Witte, D. Baltimore, The chronic myelogenous leukemia-specific P210 protein is the product of the bcr/abl hybrid gene. *Science* **233**, 212–214 (1986). doi: 10.1126/science.3460176; pmid: 3460176
31. N. P. Shah *et al*., Overriding imatinib resistance with a novel ABL kinase inhibitor. *Science* **305**, 399–401 (2004). doi: 10.1126/science.1099480; pmid: 15256671
32. T. Oda *et al*., Crkl is the major tyrosine-phosphorylated protein in neutrophils from patients with chronic myelogenous leukemia. *J. Biol. Chem.* **269**, 22925–22928 (1994). pmid: 8083188
33. A. Hamilton *et al*., BCR-ABL activity and its response to drugs can be determined in CD34+ CML stem cells by CrkL phosphorylation status using flow cytometry. *Leukemia* **20**, 1035–1039 (2006). doi: 10.1038/sj.leu.2404189; pmid: 16572205
34. Y. Deguchi *et al*., Comparison of imatinib, dasatinib, nilotinib and INNO-406 in imatinib-resistant cell lines. *Leuk. Res.* **32**, 980–983 (2008). doi: 10.1016/j.leukres.2007.11.008; pmid: 18191450
35. U. Kruse *et al*., Chemoproteomics-based kinome profiling and target deconvolution of clinical multi-kinase inhibitors in primary chronic lymphocytic leukemia cells. *Leukemia* **25**, 89–100 (2011). doi: 10.1038/leu.2010.233; pmid: 20944678
36. M. M. Savitski *et al*., Delayed fragmentation and optimized isolation width settings for improvement of protein identification and accuracy of isobaric mass tag quantification on Orbitrap-type mass spectrometers. *Anal. Chem.* **83**, 8959–8967 (2011). doi: 10.1021/ac201760x; pmid: 22017476
37. M. M. Savitski *et al*., Targeted data acquisition for improved reproducibility and robustness of proteomic mass spectrometry assays. *J. Am. Soc. Mass Spectrom.* **21**, 1668–1679 (2010). doi: 10.1016/j.jasms.2010.01.012; pmid: 20171116
38. M. M. Savitski *et al*., Measuring and managing ratio compression for accurate iTRAQ/TMT quantification. *J. Proteome Res.* **12**, 3586–3598 (2013). doi: 10.1021/pr400098r; pmid: 23768245
39. J. A. Schellman, The thermodynamics of solvent exchange. *Biopolymers* **34**, 1015–1026 (1994). doi: 10.1002/bip.360340805; pmid: 8075384
40. J. Cox, M. Mann, MaxQuant enables high peptide identification rates, individualized p.p.b.-range mass accuracies and proteome-wide protein quantification. *Nat. Biotechnol.* **26**, 1367–1372 (2008). doi: 10.1038/nbt.1511; pmid: 19029910
41. Y. Benjamini, Y. Hochberg, Controlling the false discovery rate: A practical and powerful approach to multiple testing. *J. R. Stat. Soc., B* **57**, 289–300 (1995).
42. E. Eden, R. Navon, I. Steinfeld, D. Lipson, Z. Yakhini, GOrilla: A tool for discovery and visualization of enriched GO terms in ranked gene lists. *BMC Bioinformatics* **10**, 48 (2009). doi: 10.1186/1471-2105-10-48; pmid: 19192299

ACKNOWLEDGMENTS

We thank D. Thomson for the synthesis of GSK3182571; J. Stuhlfauth for cell culture; M. Jundt, K. Kammerer, M. Klös-Hudak, M. Paulmann, I. Tögel, and T. Rudi for expert technical assistance; and F. Weisbrodt for help with the figures. We are grateful to M. Hann and G. Neubauer for discussions and support. P.N. acknowledges funding from Karolinska Institute (DPA), the Swedish Research Council (Vetenskapsrådet), and the Swedish Cancer Society (Cancerfonden). M.M.S., F.B.M.R., M.B., P.N., and G.D. conceived the project; M.M.S., F.B.M.R., T.W., D.E., D.M.M., R.J, M.B., and G.D. designed the experiments; F.B.M.R., T.W., D.E., R.B.D., R.J., and D.M.M. conducted and supervised experiments; M.M.S., F.B.M.R., H.F., T.W., M.F.S., and M.B. analyzed proteomics data; M.M.S., F.B.M.R., S.K., B.K., M.B., and P.N. contributed to the manuscript; and G.D. wrote the manuscript. P.N. and D.M.M. are cofounders and shareholders of Pelago Bioscience. B.K. is a cofounder and shareholder of OmicScouts GmbH. P.N. is the inventor of a patent (approved in the UK and pending in other districts) controlled by Pelago Biosciences AB and Evitra Proteoma AB covering the basic CETSA method. R.H. and D.M. also have associations to Pelago Bioscience AB. Mass spectrometry data are available for download at ProteomicsDB (www.proteomicsdb.org; data set identifier PRDB004185).

SUPPLEMENTARY MATERIALS

www.sciencemag.org/content/346/6205/1255784/suppl/DC1
Materials and Methods
Figs. S1 to S12
Tables S1 to S13

8 May 2014; accepted 2 September 2014
10.1126/science.1255784

Tracking cancer drugs in living cells by thermal profiling of the proteome

Mikhail M. Savitski *et al.*

Science **346**, (2014);
DOI: 10.1126/science.1255784